Annals of Materials Science & Engineering

Austin Publishing Group

Open Access Full Text Article

Review Article

Surface Bio-Functionalization of a Novel High-Performance Hydrophilic Jeffamine-Modified Fluoro-Containing Polyimide for Biomedical Applications

Teng-Yuan Lo[1], Yen-Jen Wang[1], Dean-Mo Liu[1]* and Wha-Tzong Whang[1]*

[1]Department of Materials Science and Engineering, National Chiao Tung University, Republic of China

***Corresponding author:** Dean-Mo Liu, Department of Materials Science and Engineering, National Chiao Tung University, Hsin Chu 30049, Taiwan, Republic of China

Wha-Tzong Whang, Department of Materials Science and Engineering, National Chiao Tung University, Hsin Chu 30049, Taiwan, Republic of China

Received: May 22, 2014; **Accepted:** July 27, 2014; **Published:** July 31, 2014

Abstract

A brand-new class of Jeffamine-modified fluoro-containing polyimide (6FPI-J_x series, where x is ranging from 10 to 30% by weight) was developed in this study. Existing pristine fluoro-containing polyimide (6FPI) is a flexible and high-performance polymer with low surface energy for advanced engineering applications. Although it has been considered as promising biomaterial for its good blood compatibility, it has known to be toxic to normal cells. Here, we modified 6FPI (with –C $(CF_3)_2$- group on backbone) with hydrophilic diamine monomer, Jeffamine, which denoted as 6FPI-J_x, where x is the molar percentage of the total diamines. The newly synthesized 6FPI-J_x series was systematically characterized in terms of surface properties included surface texture, chemistry, potential, and charging. Besides, the 6FPI-J_x copolymer exhibited good mechanical and stability as pristine 6FPI. With addition of Jeffamine (x=10%), 6FPI-J_{10} displayed considerably improved blood and cell compatibility compared to 6FPI, which was explainable as a combined effect of morphological texture and chemical environment of resulting surface. The new class of 6FPI-J_x exhibited excellent solubility toward a number of organic solvents, which rendered the 6FPI-J_{10} a great potential candidate as biocompatible coating for implantable medical devices and also for potential therapeutic applications.

Keywords: Fluoro-containing PI; Jeffamine; 6FPI-J_x series; Biocompatibility; Surface biofunctionalization

Introduction

Polyimide (PI) has readily been a widely-used polymeric material in industry for its outstanding properties included high mechanical strength, good electrical insulting, high thermal stability and excellent chemical resistance over many polymeric alternatives. These merits render PI a perfect candidate in high-performance engineering applications since the past decades. Till recently, PI has been proven to be a biocompatible material and promoted for biomedical applications [1-6]. For instance, PI was applied as electrodes in biosensing microdevices [2,6,7], such as the elegant work reported by S. Metz et al. who developed flexible, implantable PI microprobes that allowed simultaneous, selective chemical delivery/probing and multi-channel recording/stimulation of bioelectric activity [1]. The devices can be used to collect the chemical and electrical signals between cells in vitro and in vivo.

The introduction of fluorine atoms into PI also brings attractive features such as low water uptake, water and/or oil repellence, low dielectric constant, low refractive index, resistance to wear and abrasion, and good thermal and chemical stabilities [8], thus fluoro-containing PI has already drawn attractions from microelectronic and optoelectronic sectors. On the other hand, one of the technical advantages of fluoro-containing PI is its good miscibility with organic solvents. Previous studies also showed that fluoro-containing PI can be prepared via one-step imidization (chemical and solution imidization) [9], which allowed a shape-forming procedure to be processed under relatively low temperature compared with conventional high-temperature imidization, and the mechanical strength of such kind of PI is also guaranteed. This characteristic appears to provide technical flexibility in biomedical uses, especially when active or therapeutic molecules are simultaneously incorporated during the forming procedure. Although the work of fluoro-containing PI in the field of biomedicine was not extensively explored, there were interesting features that should provide technical and biological advantages over other polymeric candidates. Kawakami et al. reported that fluorinated polyimide showed good blood compatibility and provides the suppressions of protein adsorption, neutrophil adhesion, and complement activation [10-12]. These properties were likely contributed from the CF_3 groups on the backbone and thus the overall hydrophobicity was improved. The CF_3 groups also provided strong negative zeta potential which inhibited adhesions of some negatively charged plasma proteins such as albumin and fibrinogen [13]. Considering those aforementioned advantages, fluoro-containing PI is expected to exerting clinical potential, for example, as biocompatible or non-fouling coating for implanted devices in the areas of orthopedics, dentistry, endovascular stents, and implantable drug delivery systems. However, technical information about fluoro-containing PI in biological performance is still insufficient to support more critical application, such as its relatively high hydrophobicity and strong negative surface charging that may potentially exert adverse effects toward cells, blood or tissues. It is more biologically desirable if hydrophilic and charging character can be finely tuned in

Whang et al. © All rights reserved

Citation: Teng-Yuan L, Yen-Jen W, Dean-Mo L and Wha-Tzong W. Surface Bio-Functionalization of a Novel High-Performance Hydrophilic Jeffamine-Modified Fluoro-Containing Polyimide for Biomedical Applications. Ann J Materials Sci Eng. 2014;1(2): 8.

a control manner into the fluoro-containing PI to optimize resulting biocompatibility for a vast number of biomedical uses.

With the advancement of current biomaterials technology, it is more desirable and biomedically significant with the stringent requirement in clinical practices, a further improvement of the biocompatibility of the fluoro-containing PI was our primary concern. Here, we explore a new synthetic methodology by using a nontoxic monomer to synergize fluoro-containing PI copolymer with improved biocompatibility, while maintaining sufficient solubility to facilitate shape-forming capability. Some existing soluble PIs have been suffered from the problems of brittleness due to low reactivity between monomers and backbone structure factors. How to achieve a balance between solubility and mechanical strength is essential. In this work, polyethylene glycol (PEG) was employed as a nontoxic polymer and has been known to be highly water soluble, non-immunological, non-fouling, and compatible in medicine for years [14-17]. While PEG alone is unable to support cellular activities, many kinds of PEG-containing copolymers have been successfully investigated in vitro and in vivo, as drug delivery systems and tissue scaffolds [17]. The nonionic and hydrophilic features of PEG also guarantee good biocompatibility of PEG-containing copolymers.

Here, a combination of 6FDA-BisAAF, as the main fluoro-containing PI matrix, and diamine-terminated PEG molecule (Jeffamine), as copolymer monomer was designed. In concern of sufficient solubility and mechanical strength of the resulting PI, ratios between Jeffamine and BisAAF were carefully chosen here to ensuring the resulting copolymer that can undergo solution imidization and be mechanically flexible after casting films. The properties of Jeffamine-containing PI were experimentally verified and the comparisons between PIs with different Jeffamine ratios were made for property optimization included structure morphology, contact angle, zeta potential, surface chemistry, and cytocompatibility and blood compatibility.

Experimental

Materials

2,2'-bis-(3,4-dicarboxyphenyl) hexafluoropropane dianhydride (6FDA) and 2,2-Bis(4-aminophenyl) hexafluoropropane (BisAAF) were purchased from ChrisKev, INC. 2,2'-(Ethylenedioxy) bis(ethylamine) (Jeffamine EDR-148, denoted as Jeffamine in this paper, 97+%) and m-Cresol (99%) were obtained from Alfa Aesar. Isoquinoline (97%) was obtained from ACROS. The molecular structures of monomers employed are given in Figure 1a.

6FPI-J_x series synthesis

Four different ratios of BisAAF and Jeffamine were chosen here and the ratios were 10:0, 9:1, 8:2, and 7:3, respectively. The PI containing Jeffamine was denoted as 6FPI-J_x, where x was the molar percentage of the total diamines. The reason why we did not choose more Jeffamine additions was that when the proportions of Jeffamine exceeded 30 mol% of the total diamine, the 6FPI-J_x series precipitated in the solvent and could not undergo solution imidization. BisAAF and Jeffamine were added into 32g m-cresol and stirred until all diamines were fully dissolved. After diamines dissolving, 0.24g isoquinoline was added into the solution and the solution stirred for 1 hr at room temperature. The amount of isoquinoline was 0.3 wt% of the total solid content of the 6FPI-J_x series. 6FDA was separated into three pieces to add into the solution. The next piece of 6FDA was added until the former part was fully dissolved. When the total 6FDA was totally dissolved, the solution continued to stir for 2 hrs at room temperature. And then the solution was heated to 50-70°C and 130-150°C for 2hrs, respectively. After the two-stages of heating, the solution was stirred at 180°C for 48 hrs. When the synthesis was finished, the 6FPI-J_x series solution cooled down to room temperature and was poured into the mixed solution of water and ethanol (ratio: 1:1). The 6FPI-J_x series precipitated in the mixed solution. We collected this precipitation and washed them for two times in mixed solution of water and ethanol to make sure that left m-cresol was washed out from precipitation. The 6FPI-J_x series precipitation was then baked at 110°C under vacuum atmosphere for 24 hrs to remove ethanol and water. This dried 6FPI-J_x series can be redissloved to organic solvent to perform coating. Figure 1b shows a highly foldable 6FPI-J_{10} film (as a representative sample), ensuring the film possessed high flexibility and sufficient mechanical strength. Surface coating on metal was performed by dipping stainless steel 304 rod into *tetrahydrofuran* (THF) solution containing 20wt% 6FPI-J_x and then dried at room temperature.

Fourier transforms infrared spectroscopy

The Fourier transform infrared spectroscopy (FTIR) spectra of 6FDA-BisAAF and 6FPI-J_x series were obtained by Fourier transform infrared spectrometer (FTIR, Perkin Elmer Spectrum 100 Optica). The spectra were obtained with 64 scans for each sample under N_2 atmosphere. The scan range of IR spectra was from 450 cm^{-1} to 4000 cm^{-1}.

Atomic force microscopy

Atomic Force Microscopy (AFM, Innova Scanning Probe Microscope) was used for deriving the surface roughness profile and phase distributions. All the measurements were performed in a dry environment at room temperature in tapping mode over a sampling area of 3 × 3 μm^2 for 6FDA-BisAAF and 6FPI-J_x series, respectively. The images had a resolution of 512 × 512 pixels and were acquired at a scanning rate of about 0.5 Hz. The images obtained were processed with the diSPMLab software (Veeco).

Electron spectroscopy for chemical analysis

The surface chemistry of 6FDA-BisAAF and 6FPI-J_x series films

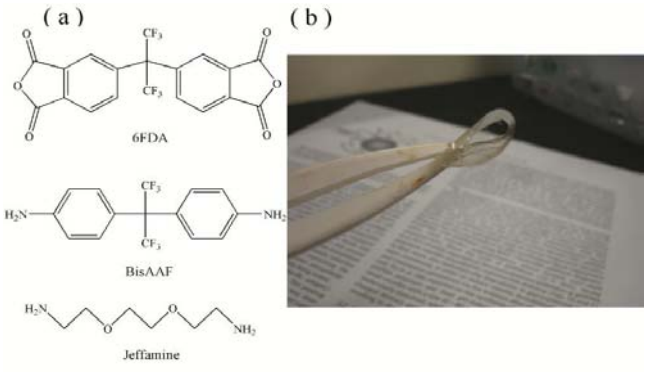

Figure 1: (a) The monomers structures used in 6FPI-J_x series synthesis. (b) The 6FPI-J_{10} membrane can be easily folded, showing good mechanical flexibility.

was characterized by Electron Spectroscopy for Chemical Analysis (ESCA, Ulvac-PHI PHI 1600) with 15 kV Al/Mg X-ray source. In this study, all the ESCA measurements were performed by using Mg K_α emission at 1253.6 eV. A single survey scan spectrum (0–1100 eV) and narrow scans for C1s (280–300 eV) were recorded for each sample with a pass energy of 1 and 0.1 eV, respectively. Background was subtracted by using the Shirley formula. The deconvolution was done by fitting the spectra to multiple peaks comprised of a Gaussian function. The charge effect was compensated by setting the binding energy of aromatic carbons, which does not link to oxygen or nitrogen, at 285.0 eV.

Contact angle measurement

Contact angles of water on PIs were examined by using a contact angle meter which was also used in previous published research [18]. Surface wetting ability of the samples was determined by measuring the water contact angle with one drop (5 µl) of deionized water using a contact angle meter at room temperature. Six measurements were performed on each sample to evaluate the average contact angle θ, at 5 s.

Membrane zeta potential measurement

Measurements via a streaming potential apparatus were carried out with 0.01 M aqueous KCl solution with pH=7, at four pressure differences ranging from 0.1 to 0.6 MPa. The zeta potential was given by the Helmholtz–Smoluchowski equation with the Fairbrother and Mastin approach [19]:

$$\zeta = \Delta E \eta \kappa / \Delta P \, \varepsilon \, \varepsilon_0$$

where ζ is the zeta potential, ΔE is the streaming potential, ΔP is the applied pressure, η is the viscosity of the solution, κ is the solution conductivity, ε and ε_0 are the permittivity of the test solution and free space, respectively.

Cytotoxicity assay

A10 vascular smooth muscle cells (VSMCs) from Food Industry Research and Development Institute (Hsinchu, Taiwan) were cultured in DMEM supplemented with 10% fetal bovine serum and 1% antibiotic antimycotic solution (Gibco, USA) in a humidified atmosphere containing 5% CO_2 in air at 37°C. The investigation of cell viability is a common method to evaluate the biocompatibility of biomaterials. The cytotoxicity of 6FDA-BisAAF and 6FPI-J_x series was evaluated using VSMCs by MTT colorimetric procedure. VSMCs were plated at 2 x 10^4 cells per well in a 24-well culture plate (Corning, USA) for 48 h to attach, followed by replacement of the sample solutions and incubation for a predetermined time. At a predetermined time, the medium containing samples was aspirated and the wells were washed twice using PBS solution. Then, MTT solution (0.5 mg/mL) was added and incubated for 4 h. The purple formazan was solubilized with isopropanol and measured in a microplate reader (GDV model DV 990 BV4, Italy) at 595 nm.

Activated partial thromboplastin time

For the activated partial thromboplastin time (APTT) measurements, the 6FDA-BisAAF and 6FPI-J_x series were put into a special test tube. The 100 µl fresh human platelet-poor-plasma (PPP) was obtained by centrifuging the whole blood at 3000 rpm. 100 µl actin-activated cephthaloplastin reagent were then added into the above tube containing 6FDA-BisAAF and 6FPI-J_x series, followed by the addition of a 0.03 M Actin FSL $CaCl_2$ solution (100 µl) after 3 min incubation at 37°C. We used a coagulometer (CA-50, Sysmex) to measure the clotting time of the plasma solution.

Results and Discussion

Structural analysis

Figure 2 shows the FT-IR spectra of 6FPI-J_x series with different Jeffamine ratios. The typical characteristic peaks designated to PI at 1780 cm^{-1} (C=O asymmetrical stretching), 1720 cm^{-1} (C=O symmetrical stretching), 1380 cm^{-1}(C-N stretch) and 1550 cm^{-1} (C-NH of polyamic acid) were absent [20], indicating that the 6FPI-J_x series were fully imidized through the synthesis. With increasing Jeffamine addition, two peaks (2939 and 2870 cm^{-1}, designated as CH_2-O asymmetric and symmetric stretches, respectively) appeared and their intensity increased with increasing Jeffamine concentration [21]. However, no detectable peak of alkyl ether group near 1120 cm^{-1} in the full range spectrum was found [22], suggesting the interferences resulting from the 6FDA-based polyimide which has native peaks at 1104 (imide band) and 1140 cm^{-1}(C-F stretching) [23-25]. Figure 3 shows the FTIR deconvoluted spectrum of 6FPI-J_{30} from 1090 to 1160 cm^{-1}, wherein the ether peaks at 1123 cm^{-1} was lying between 1102 (imide band) and 1144 cm^{-1} (C-F stretching). Since the fluorinated monomers were the main monomers, the peak of alkyl ether signal could not be observed because of the strong absorbance of 6FDA-BisAAF native function groups. According to FTIR spectra, the 6FPI-J_x series remained structurally stable even after dissolution in organic solvent such as DMAC and THF during film casting process indicating the newly-formed 6FPI-J_x provided a wider and milder processability.

Surface characterization

The surface structure of the 6FDA-BisAAF and 6FPI-J_x series was

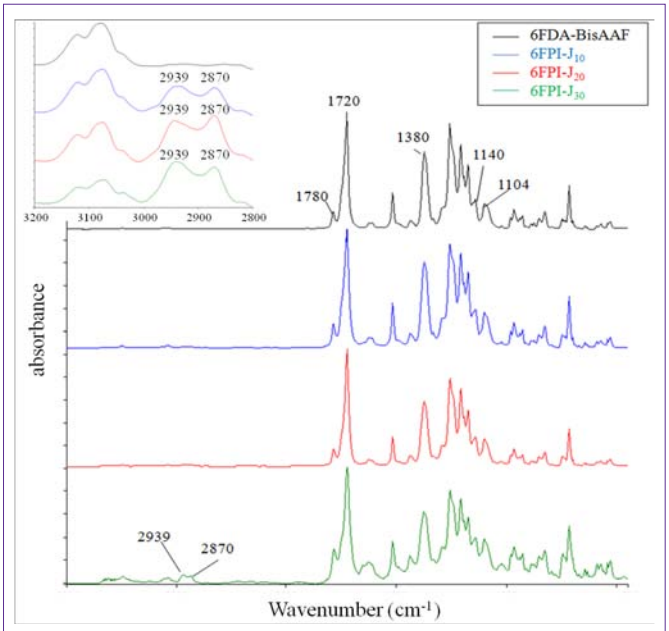

Figure 2: The FT-IR absorbance spectrum of 6FDA-BisAAF and 6FPI-J_x series. The characteristic peaks of 6FDA-BisAAF and 6FPI-J_x series are labeled in this figure. Left top sub-spectrum shows the absorbance of CH_2-O asymmetric (2939 cm^{-1}) and symmetric stretches (2870 cm^{-1}) of 6FPI-J_x series. These two peaks are absent in 6FDA-BisAAF curve.

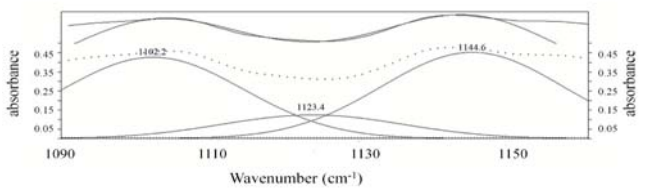

Figure 3: The deconvolution FTIR spectrum of 6FPI-J_{30} from 1090 cm^{-1} to 1160 cm^{-1}.

examined using AFM, as shown in Figure 4 and Table 1. The surface prepared with 6FDA-BisAAF showed a very smooth morphology with R_a (average roughness) = 0.377 nm and R_q (route mean square roughness) = 0.476 nm. For 6FPI-J_x series, Table 1 gives that R_a and R_q gradually increased as the Jeffamine increased. The surface remained flat until Jeffamine reached 20%, above which a number of grooves of several hundred nm width appeared. When Jeffamine concentration reached 30%, there was a noticeable enhancement of roughness (R_a=1.46 nm and R_q=2.68 nm) for 6FPI-J_{30} compared to other samples. The 6FPI-J_{30} showed a surface texture with randomly distributed "hills" of height range of 20~50 nm, giving rise to enhanced roughness. The roughness was increasing with the amount of Jeffamine addition and to specify what caused the change in surface textures, we adopted phase images as supporting information to elucidate the evolution of copolymer surface.

Figure 5 illustrates the phase diagram of 6FDA-BisAAF and 6FPI-J_x series, wherein the brighter regions in the diagram represented softer phases of surfaces. The phase signal changed when the probe encountered regions of different compositions. Phase shifts corresponded to the changes of mechanical properties of sample surface. In principle, when oscillating cantilever interacts with softer regions of surface, more changes in the cantilever's deflection or vibration amplitude lead to stronger shifts in phase angle, reflecting as the brighter regions. Phase contrast generates by transforming the changes in phase lag to bright and dark regions in phase images. When Jeffamine ratio was increased to 10%, the bright spots distributed uniformly throughout the surface, ensuring smooth morphology, similar to that of 6FDA-BisAAF sample, Figure 5a. The brighter regions corresponded to PI segments containing Jeffamine since

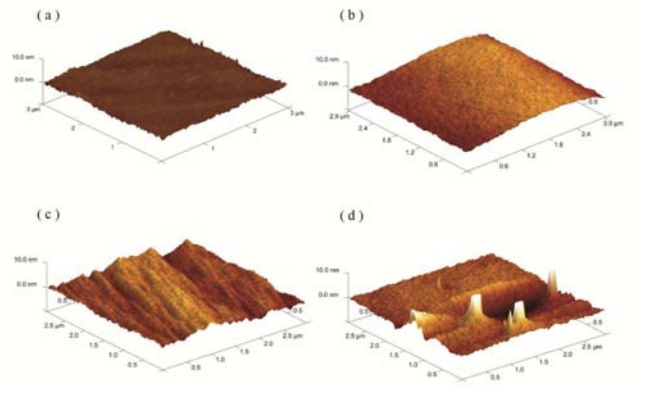

Figure 4: The AFM surface morphology spectrums of (a) 6FDA-BisAAF; (b) 6FPI-J_{10}; (c) 6FPI-J_{20}; (d) 6FPI-J_{30}. The scan area was 3x3 μm^2 and z axis range was 10 nm.

Table 1: The average roughness (R_a), root-mean-squared roughness (R_q) and maximum height (R_{max})values of 6FDA-BisAAF and 6FPI-J_x series.

	R_a	R_q	R_{max}
6FDA-BisAAF	0.377 nm	0.476 nm	5.59 nm
6FPI-J_{10}	0.753 nm	0.973 nm	6.49 nm
6FPI-J_{20}	0.914 nm	1.13 nm	7.15 nm
6FPI-J_{30}	1.46 nm	2.68 nm	53.3 nm

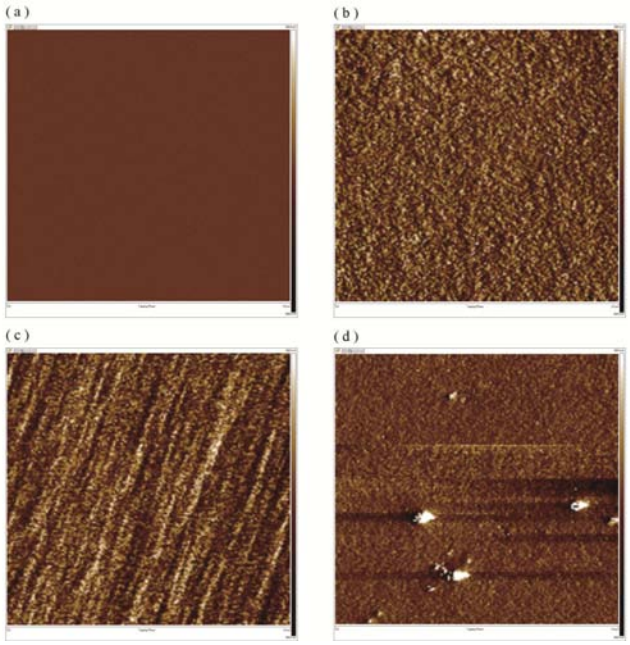

Figure 5: The AFM phase diagrams of (a) 6FDA-BisAAF; (b) 6FPI-J_{10}; (c) 6FPI-J_{20}; (d) 6FPI-J_{30}.

Jeffamine possesses ether backbones, which are mechanically softer than aromatic backbones. The 6FPI-J_x series exhibited softer main chains than that of fluorinated monomers, but poorer solubility. The reason that the roughness increase could come from the decreased solubility of 6FPI-J_x series compared to fluoro-containing PI. When ether groups were incorporated into fluoro-containing PI backbones, since ether groups were not bulky in volume, the segment containing ether groups showed poorer solubility toward organic solvent [26]. These segments with ether backbones "precipitated" first on resulting surface upon film formation, leading to phase separations. For 6FPI-J_x series containing above 10% Jeffamine, surface textures including grooves and hills in Figure 4c-d, matched the bright regions displayed in Figure 5c-d, further confirming that the PEG-containing segments of 6FPI-J_x generated new phase from the native PI matrix. As Jeffamine addition increased, these precipitations caused more phase separation as was observed from AFM images and phase diagrams. Combining those technical data from surface texture and phase images, ether-containing phases generated more pronounced topological textures as Jeffamine ratio increased. For higher Jeffamine ratios, the surface structure became more morphologically heterogeneous as a result of aggregation, leading to grooves and hills texture and thus increased surface roughness.

Surface chemistry

The profile of the chemical bonding on the surface of 6FDA-

BisAAF and 6FPI-J_x series is given in Table 2. After Jeffamine was added, the O 1s proportion from 10.64% to 13% and remained unchanged as the Jeffamine ratios increased. There had a drop in concentration of F 1s spectrum for 6FPI-J_{10} and then increased to 11.17 atomic percent as Jeffamine ratio reached 20%. For 6FPI-J_{30}, F 1s atomic percent decreased to 6.70% but was still higher than that of 6FPI-J_{10}. Figure 6 shows the C 1s spectrums of 6FPI-J_x series with several ratios of Jeffamine addition. Figure 6a indicates that the split peaks from C 1S signal of 6FDA-BisAAF were C-C (285 eV), C-N (286.2 eV), C=O (288.6 eV) and CF_3 (293 eV), respectively [27,28]. When Jeffamine addition ratio reached 10%, the C-O signal coming from the ether groups of Jeffamine backbone appeared at 286.5 eV in Figure 6b. The CF_3 signal decreased significantly compared to that of 6FDA-BisAAF. As Jeffamine ratio reached 20%, the intensity of CF_3 signal increased but the intensity of C-O remained almost unchanged. For 6FPI-J_{30} the signal of CF_3 became slightly weak and there was still no measurable increase of C-O peak intensity. Table 3 shows the area proportions of deconvoluted binding peaks of C 1s signal for 6FPI-J_x series. The changes in CF_3 signal matched the F 1s atomic proportions on the surfaces. The C-O proportion of 6FPI-J_{10} was slightly higher than others but there was no direct correlation over different Jeffamine additions.

It is concluded, from current ESCA analysis, that with low Jeffamine addition, the intensity of CF_3 groups was suppressed by the introduction of ether group and thus hydrophilicity of 6FPI-J_x series increased. As Jeffamine ratio increased to 20% and 30%, there was no appreciable variation in intensity of ether groups. Ether groups are hydrophilic and thermodynamically unfavorable to expose as part of surface structure due to surface energy concern. Since air was considered to be hydrophobic environment, more hydrophobic groups like CF_3 are preferred to evolving as segregating phase on top of the surface instead of ether groups during film formation. On the other hand, the Jeffamine-containing phases were randomly distributed throughout sample surface from AFM exanimation. Aggregation of Jeffamine-containing phase increased with Jeffamine, i.e., for 6FPI-J_x with x > 20, and transformed homogeneous 6FDA-BisAAF surface to heterogeneous one. Randomly distributed surface textures caused by Jeffamine-containing phases could interfere with the detection accuracy on the distribution of functional groups along the surface since ESCA has a detection limitation over a length below 50Å from top surface. However, since hill-like textures on 6FPI-J_{30} surface tends to be more easily detected compared to flat region of the 6FDA-BisAAF phase, such a discrepancy may cause a potential risk of measuring error in estimation of the correlation between analytical results and real Jeffamine addition ratios.

Table 2: The surface element atomic proportions of 6FDA-BisAAF and 6FPI-J_x series.

	C 1s	N 1s	O 1s	F 1s
6FDA-BisAAF	74.09%	2.86%	10.63%	12.42%
6FPI-J_{10}	79.78%	2.40%	13.04%	4.78%
6FPI-J_{20}	73.54%	3.71%	11.57%	11.17%
6FPI-J_{30}	77.97%	2.26%	13.06%	6.70%

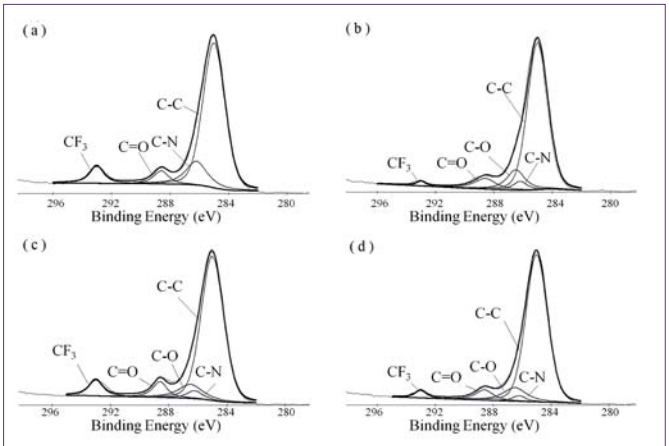

Figure 6: The C 1s ESCA spectrums of (a) 6FDA-BisAAF; (b) 6FPI-J_{10}; (c) 6FPI-J_{20}; (d) 6FPI-J_{30}. The deconvoluted binding peaks of C 1s are labeled in each sub-figure. The split peaks from C 1s signal of 6FDA-BisAAF and 6FPI-J_x series were C-C (285 eV), C-N (286.2 eV), C-O (286.5 eV), C=O (288.6 eV) and CF_3 (293 eV), respectively.

Table 3: ESCA bindings and relative peak area percentages of deconvoluted C 1s spectra obtained from 6FDA-BisAAF and 6FPI-J_x series.

	C-C	C-N	C-O	C=O	CF_3
6FDA-BisAAF	72.63%	14.68%	0%	5.69%	7.00%
6FPI-J_{10}	75.20%	4.9%	11.82%	7.49%	1.40%
6FPI-J_{20}	73.39%	3.65%	9.93%	6.53%	6.50%
6FPI-J_{30}	79.97%	2.43%	10.23%	5.90%	2.69%

Contact angle

From those aforementioned measurements, it is expected that both the textural variation and hydrophobicity of the resulting surface will affect the contact behavior of biological substances such as blood, cells, proteins etc. Here, we first conducted a measurement on contact angle with water droplet. Table 4 gives the contact angle of 6FDA-BisAAF and 6FPI-J_x series. As expected, 6FDA-BisAAF exhibited hydrophobic feature with a high contact angle of 80.34 ± 1.60°. With different amounts of Jeffamine coordinated into the fluorinated PI matrix, 6FPI-J_{10} showed slight enhancement in hydrophilicity with a contact angle of 78.29 ± 0.68°. However, the contact angles of 6FPI-J_x series were slightly increased and reached to that of 6FDA-BisAAF (80.32 ± 0.54° for 6FPI-J_{30}) when 30% of Jeffamine was incorporated. The change in contact angle was not significant even we deployed more Jeffamine in our synthesis. 6FPI-J_x series with increasing Jeffamine ratios did not show increasing wetting ability. We inferred that the variation in wetting ability of the resulting 6FPI-J_x should result from the changes of surface chemistry and surface roughness (textural variation). Even ESCA results showed that 6FPI-J_{10} exhibited lowest CF_3 and highest C-O signal, the increase in hydrophilicity was not obvious as we predicted. When Jeffamine concentration further increased, the increase in contact angle might contribute from the increase of surface roughness according to topological examination with AFM.

Table 4: Contact angle values of 6FDA-BisAAF and 6FPI-J_x series.

	Contact angle (degree)
6FDA-BisAAF	80.34 ± 1.60
6FPI-J_{10}	78.29 ± 0.68
6FPI-J_{20}	79.05 ± 0.77
6FPI-J_{30}	80.32 ± 0.54

Zeta potential

Besides the chemistry and energy distribution of the resulting surface, surface charge has been well-recognized to play a major role in manipulating the behavior of cells and biomolecules in host. According to Kawakami et al. [10-12], 6FDA-BisAAF illustrated a strong negative zeta potential and further decreased as curing temperature increased. For the new compositions developed in this work, Table 5 indicates a reduction of zeta potential to -5.26 mV for 6FPI-J_{10} after Jeffamine was incorporated (10%). In other words, the zeta potential of 6FPI-J_x series was approaching neutrality after small proportion of Jeffamine was added. For the case of 6FPI-J_{30}, zeta potential was turning into positive value (4.64 mV). Such a variation in fine tuning the surface zeta potential may provide advantages for optimization of surface-host interactions upon practical biomedical applications. Previous study of PEG-PLGA copolymer also indicated a variation of surface charge from negatively-charged polymers to positive zeta potential while increasing PEG ratios in co-polymer synthesis [29]. The change in surface charge for 6FPI-J_x is believed due to the complexes formation of polyether that might interact with alkali metal ion like Na^+ and K^+ in the aqueous solution, as being described in literature [30-32]. Since zeta potential measurements were performed in KCl solution and thus hydrophilic ether backbones were preferentially appeared on surface. The interaction between K^+ and the ether groups could explain the decrease in surface charge and as the Jeffamine ratios increased, the surface potential further transformed to positively charge for 6FPI-J_{30}.

In vitro cytocompatibility

The cytocompatibility of the 6FDA-BisAAF and 6FPI-J_x series toward VSMCs was evaluated by the MTT assay. 6FDA-BisAAF and 6FPI-J_x series were incubated with VSMCs for 48 hrs. Figure 7a shows that the cell viability for 6FDA-BisAAF was 74.3 ± 2.43% after 48 hours. However, for 6FPI-J_{10}, cell viability remained nearly 100% (100.94 ± 2.50%), indicating that the 6FPI-J_{10} exhibited excellent cytocompatibility toward VSMCs. In other words, the cytocompatibility of 6FDA-BisAAF can be considerably improved by addition of Jeffamine. However, further increase in Jeffamine ratios did not retain the cytocompatibility, adversely, cell viability gradually decreased, for instance, below 85% (84.82 ± 1.68%) when Jeffamine ratio reached 30%. However, the cell viability of the 6FPI-J_{30} was still higher than that of the 6FDA-BisAAF. This finding indicated that the outstanding cytocompatibility of the 6FPI-J_x series can be optimized with small incorporation of Jeffamine. Figure 7b-c shows the optical microscopy image of VSMC as a control and in the presence of 6FPI-J_{10}. The VSMC remained unchanged in its cellular geometry on 6FPI-J_{10} as that on the control set. The white spots represented dead VSMC nucleuses. Although dead VSMC nucleuses on 6FPI-J_{10} were more than that of the control, 6FPI-J_{10} still exhibited very nice cell viability performance as the control, indicating VSMC proliferated very well on 6FPI-J_{10}.

Table 5: Zeta potential values of 6FDA-BisAAF, 6FPI-J_{10} and 6FPI-J_{30} membranes.

	Zeta potential (mV)
6FDA-BisAAF	-42~-64 [11]
6FPI-J_{10}	-5.26
6FPI-J_{30}	4.64

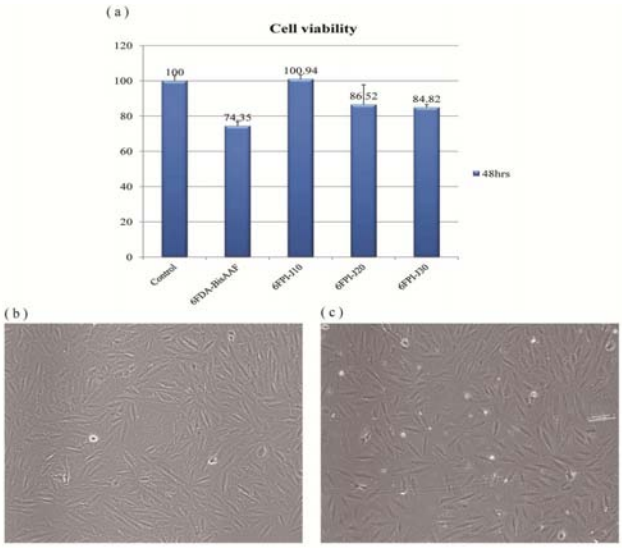

Figure 7: (a) The VSMC cell viability of 6FDA-BisAAF and 6FPI-J_x series after 48 hrs. Each data point is represented as mean ± SD (n = 3). The optical microscopy images show VSMC cellular geometry on (b) control; (c) 6FPI-J_{10}.

Factors like wetting ability and surface roughness had been well-known to give great impact on cell attachment and proliferation [33-38]. From ESCA and AFM examinations, the wetting ability of the 6FPI-J_x was inferred from a combination of textural roughness and chemical environment of the surface. From current observation, VSMC could react differently on 6FPI-J_x series even though the scale of surface roughness (in nanometric length) was much smaller compared to cell dimension. Considering roughness issue, randomly distributed topology caused by phase separations seemed to have great impacts on VSMC adhesion and proliferation. The smoother and more hydrophilic surfaces of 6FPI-J_{10} performed well in in-vitro tests. Surface charge will be another important factor, strong negative charge of 6FDA-BisAAF led to poor cell adhesion since VSMC had slightly negative charge. For 6FPI-J_x series, no direct correlations can be established between zeta potentials and cell viability since the zeta potentials of 6FPI-J_x series closed to neutrality. Although it is hard to give a precise and quantitative estimation on the surface-induced cellular behavior in this preliminary investigation, the variation of surface properties for the 6FPI-J_x as a function of Jeffamine was essential for a responsive cellular behavior and can be selectively employed for specific applications.

Blood compatibility

The APTT test is widely-used standard protocol for the clinical detection of abnormality of blood plasma and for the primary screening of the anticoagulative chemicals. The control APTT time for a healthy blood plasma was regarded to be about 39.5 ± 1.1s (Figure 8). The APTT of 6FDA-BisAAF was 40.3 ± 0.28s and showed that fluoro-containing PI had good blood compatibility as previous work reported [10-13]. When the blood plasma was incubated with 6FPI-J_{10}, the APTT were increased to 40.8 ± 2.12s, indicating that addition of Jeffamine improved the blood compatibility comparing with fluoro-containing PI. When the blood plasma was incubated with 6FPI-J_x series with higher percentage of Jeffamine, the APTT gradually increased as Jeffamine proportionally increased. APTT was

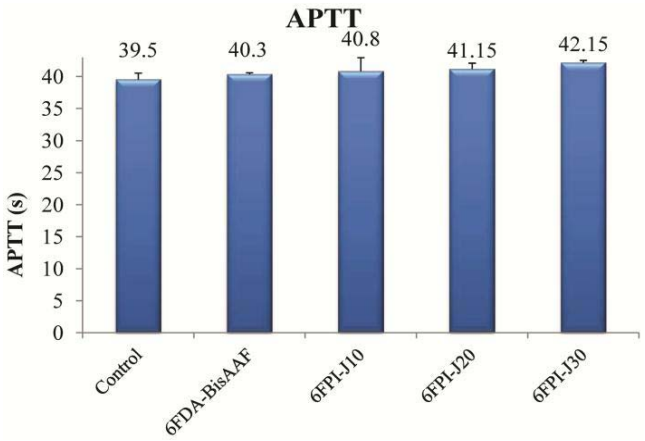

Figure 8: APTT results of 6FDA-BisAAF and 6FPI-J_x series. Each data point is represented as mean ± SD (n = 3).

further prolonged to 42.15 ± 0.35s for 6FPI-J_{30}, indicating ether group can prolong the occurrence of intrinsic pathway system. Therefore, incorporating Jeffamine addition should play an important role in inhibiting the activities of some clotting factors of blood plasma involved in APTT.

The improvements in blood compatibility exhibited an increasing trend with increasing Jeffamine addition. The strong negativity of 6FDA-BisAAF was the main factor contributing to the anti-protein adsorption, leading to good blood compatibility [10-13]. With increasing Jeffamine ratios, the zeta potentials decreased, the contribution from surface charges became less pronounced, likewise, PEG copolymers exhibited less thrombogenic feature, due to the flexibility and hydrophilicity of the backbone [39]. From current experimental observation, we believed that the improvement in blood compatibility in 6FPI-J_x was contributed from the ether backbones of the Jeffamine monomers.

Figure 9a shows the SEM images of 6FPI-J_{10} coating on stainless steel 304 rod. The whole coating process was carried out at room temperature. In Figure 9a we can clearly see that 6FPI-J_{10} coating smoothly covered the whole rod surface. The magnified image of 6FPI-J_{10} coating which placed in top-right corner of Figure 9a further proofed the flatness and homogeneity of the surface coating as AFM results showed. These SEM images indicated the capability of 6FPI-J_x as biocompatible coating on metal implant. Furthermore, the surface chemistry can also be tuned by soaking 6FPI-J_x in 1M KOH aqueous solution. Figure 9b shows the FTIR spectrum of pristine and base-treated 6FPI-J_x. According to previous lecture, surface imide content can obtained by calculating the ratio between peak intensity at 1720 cm^{-1} (C=O symmetric stretching) and peak intensity at 1500 cm^{-1} (benzene peak) [40]. The relative surface imide content of untreated 6FPI-J_x was set as 100%. After immersing in KOH aqueous solution for 30 min, the signal of aromatic ring at 1500 cm^{-1} remained unchanged but the peak intensity at 1720 cm^{-1} greatly dropped. Thus we could obtain the relative imide content of treated 6FPI-J_x by comparing peak intensity at 1720 cm^{-1}. The absorption intensities at 1720 cm^{-1} were 2.6 and 1.08 for pristine and base-treated 6FPI-J_x, respectively. We found the relative imide content of base-treated 6FPI-J_x dropped to 41.54%, indicating part of imide groups were cleaved to form carboxylic acids and amide groups. According to the lecture published

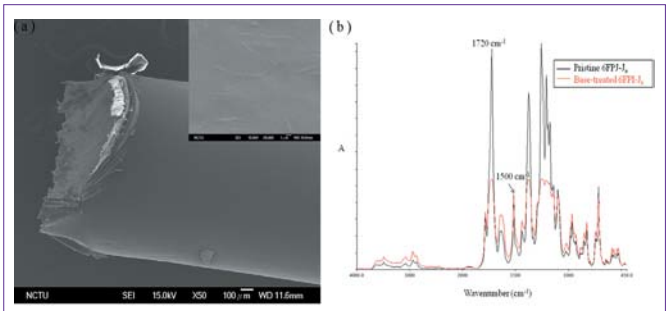

Figure 9: (a) SEM image of 6FPI-J_{10} coated stainless steel 304 rod. The top-right sub-image is the magnified image of 6FPI-J_{10} surface. (b) FTIR spectrum of pristine and base-treated 6FPI-J_x films.

by our group, base treatment rendered the tunable surface chemistry for further modification such as metalization [40]. We believed this biocompatible 6FPI-J_x had good potential for biomedical application such as implant coating and flexible bioelectric uses.

Conclusion

We have successfully synthesized the Jeffamine-containing 6FPI-J_x series in this work. The 6FPI-J_x series exhibited good mechanical flexibility and excellent solubility toward organic solvent. With proper addition of hydrophilic Jeffamine, considerable improvement in cell and blood compatibility was observed. By optimizing Jeffamine addition, 6FPI-J_{10} exhibited moderate hydrophilicity and smoother surface, which facilitated VSMC adhesion and proliferation. Considering the factors manipulated the surface properties, this newly-synthesized 6FPI-J_x co-polymer envisioned a great potential as a new class of biomaterials for particularly coating applications toward a vast number of implantable medical devices. Its milder processing and forming capability compared to existing synthesis alternatives permits a potential incorporation of therapeutic or vulnerable molecules for multifunctional practices, and is currently under investigation.

Acknowledgement

This project is supported by Ministry of Science and Technology, Taiwan, under Contract No. NSC 100-2221-E-009-023-MY3 and MOST 103-2221-E-009-216.

References

1. Metz S, Bertsch A, Bertrand D, Renaud P. Flexible polyimide probes with microelectrodes and embedded microfluidic channels for simultaneous drug delivery and multi-channel monitoring of bioelectric activity. Biosens Bioelectron. 2004; 19: 1309-1318.

2. Melnik E, Bruck R, Hainberger R, Lämmerhofer M. Multi-step surface functionalization of polyimide based evanescent wave photonic biosensors and application for DNA hybridization by Mach-Zehnder interferometer. Anal Chim Acta. 2011; 699: 206-215.

3. Rubehn B, Stieglitz T. In vitro evaluation of the long-term stability of polyimide as a material for neural implants. Biomaterials. 2010; 31: 3449-3458.

4. Myllymaa S, Myllymaa K, Korhonen H, Lammi MJ, Tiitu V, Lappalainen R, et al. Surface characterization and in vitro biocompatibility assessment of photosensitive polyimide films. Colloids Surf B Biointerfaces. 2010; 76: 505-511.

5. Julien S, Peters T, Ziemssen F, Arango-Gonzalez B, Beck S, Thielecke H, et al. Implantation of ultrathin, biofunctionalized polyimide membranes into the subretinal space of rats. Biomaterials. 2011; 32: 3890-3898.

6. Prichard HL, Reichert WM, Klitzman B. Adult adipose-derived stem cell attachment to biomaterials. Biomaterials. 2007; 28: 936-946.

7. Bruck R, Melnik E, Muellner P, Hainberger R, Lammerhofer M. Integrated polymer-based Mach-Zehnder interferometer label-free streptavidin biosensor compatible with injection molding. Biosens Bioelectron. 2011; 26: 3832-3837.

8. Hougham G, Tesoro G, Shaw J. Synthesis and properties of highly fluorinated polyimides. Macromolecules 1994; 27: 3642-3649.

9. Qiu Z, Wang J, Zhang Q, Zhang S, Ding M, Gao L. Synthesis and properties of soluble polyimides based on isomeric ditrifluoromethyl substituted 1,4-bis(4-aminophenoxy)benzene. Polymer 2006; 47: 8444-8452.

10. Kawakami H. Polymeric membrane materials for artificial organs. J Artif Organs. 2008; 11: 177-181.

11. Kawakami H, Kanno M, Nagaoka S, Kubota S. Competitive plasma protein adsorption onto fluorinated polyimide surfaces. J Biomed Mater Res A. 2003; 67: 1393-1400.

12. Nagaoka S, Kanno M, Kawakami H, Kubota S. Evaluation of blood compatibility of fluorinated polyimide by immunolabeling assay. J Artif Organs 2001; 4: 107-112.

13. Kanno M, Kawakami H, Nagaoka S, Kubota S. Biocompatibility of fluorinated polyimide. J Biomed Mater Res. 2002; 60: 53-60.

14. Nakayama Y, Miyamura M, Hirano Y, Goto K, Matsuda T. Preparation of poly(ethylene glycol)-polystyrene block copolymers using photochemistry of dithiocarbamate as a reduced cell-adhesive coating material. Biomaterials. 1999; 20: 963-970.

15. Park D, Wu W, Wang Y. A functionalizable reverse thermal gel based on a polyurethane/PEG block copolymer. Biomaterials. 2011; 32: 777-786.

16. Kim SH, Tan JP, Fukushima K, Nederberg F, Yang YY, Waymouth RM, et al. Thermoresponsive nanostructured polycarbonate blocks copolymers as biodegradable therapeutic delivery carriers. Biomaterials. 2011; 32: 5505-5514.

17. Zivanovic S, Li J, Davidson PM, Kit K. Physical, mechanical, and antibacterial properties of chitosan/PEO blend films. Biomacromolecules. 2007; 8: 1505-1510.

18. Tsai MH, Huang YC, Tseng IH, Yu HP, Lin YK, Huang SL. Thermal and mechanical properties of polyimide/nano-silica hybrid films. Thin Solid Film 2011; 519: 5238-5242.

19. Childress AE, Elimelech M. Effect of solution chemistry on the surface charge of polymeric reverse osmosis and nanofiltration membranes. J Membr Sci. 1996; 119: 253-268.

20. Saeed MB, Zhan M-S. Adhesive strength of partially imidized thermoplastic polyimide films in bonded joints. Int J Adhes Adhes. 2007; 27: 9-19.

21. Severcan F, Toyran N, Kaptan N, Turan B. Fourier transform infrared study of the effect of diabetes on rat liver and heart tissues in the CH region. Talanta. 2000; 53: 55-59.

22. Nagarajan S, Sudhakar S, Srinivasan KSV. Poly (ethylene glycol) block copolymers by redox process: kinetics, synthesis and characterization: Pure Appl Chem. 1998; 70: 1245-1248.

23. Xiao S, Feng X, Huang RYM. Synthesis and properties of 6FDA-MDA copolyimide membranes: effects of diamines and dianhydrides on gas separation and pervaporation properties. Macromol Chem Phys. 2007; 208: 2665-2676.

24. Choi JK, Cho K, Yoon TH. Synthesis and characterization of polyimides from triphenylamine-based diamine monomers with thiophene or trifluoromethyl side group. Synthetic Metals. 2010; 160: 1938-1944.

25. Sen SK, Maji S, Dasgupta B, Chatterjee S, Banerjee S. Organosoluble poly(ether imide)s from phthalimidine based and trifluoromethyl substituted bis(ether amine). J Appl Polym Sci. 2009; 113: 1550-1559.

26. Wang C, Zhao X, Li G, Jiang J. High solubility and optical transparency of novel polyimides containing 3,3',5,5'-tetramethyl pendant groups and 4-tert-butyltoluene moiety. Polym Degrad Stabil. 2009; 94: 1526-1532.

27. Yang CY, Chen JS, Hsu SLC. Effects of O2 and N2 plasma treatment on 6FDA-BisAAF fluorine-contained polyimide. J Electrochem Soc. 2006; 153: 120-125.

28. Yang CY, Chen JS, Hsu SLC. Investigation of the interfacial reaction between metal and fluorine-contained polyimides. J Vac Sci Technol A. 2005; 23: 862-868.

29. Quesnel R, Hildgen P. Synthesis of PLA-b-PEG multiblock copolymers for stealth drug carrier preparation. Molecules. 2005; 10: 98-104.

30. Wright PV. Electrical conductivity in ionic complexes of poly(ethylene oxide). Brit Polym J. 1975; 7: 319-327.

31. Ananthapadmanabhan KP, Goddard ED. Aqueous biphase formation in polyethylene oxide-inorganic salt systems. Langmuir. 1987; 3: 25-31.

32. Chen J, Spear SK, Huddleston JG, Rogers RD. Polyethylene glycol and solutions of polyethylene glycol as green reaction media. Green Chem. 2005; 7: 64-82.

33. Saito T, Hayashi H, Kameyama T, Hishida M, Nagai K, Teraoka K, et al. Suppressed proliferation of mouse osteoblast-like cells by a rough-surfaced substrate leads to low differentiation and mineralization. Mater Sci Eng C. 2010; 30: 1-7.

34. Postiglione L, Di Domenico G, Ramaglia L, Montagnani S, Salzano S, Di Meglio F, et al. Behavior of SaOS-2 cells cultured on different titanium surfaces. J Dent Res. 2003; 82: 692-696.

35. Mitik-Dineva N, Wang J, Truong VK, Stoddart P, Malherbe F, Crawford RJ, et al. Escherichia coli, Pseudomonas aeruginosa, and Staphylococcus aureus attachment patterns on glass surfaces with nanoscale roughness. Curr Microbiol. 2009; 58: 268-273.

36. Khan SP, Auner GG, Newaz GM. Influence of nanoscale surface roughness on neural cell attachment on silicon. Nanomedicine. 2005; 1: 125-129.

37. Brunetti V, Maiorano G, Rizzello L, Sorce B, Sabella S, Cingolani R, et al. Neurons sense nanoscale roughness with nanometer sensitivity. Proc Natl Acad Sci U S A. 2010; 107: 6264-6269.

38. Ivanova EP, Truong VK, Wang JY, Berndt CC, Jones RT, Yusuf II, et al. Impact of nanoscale roughness of titanium thin film surfaces on bacterial retention. Langmuir. 2010; 26: 1973-1982.

39. Elbert DL, Hubbell JA. Surface treatments of polymers for biocompatibility. Annu Rev Mater Sci.1996; 26: 365-394.

40. Hsiao YS, Whang WT, Wu SC, Chaung KR. Chemical formation of palladium-free surface-nickelized polyimide film for flexible electronics. Thin Solid Film. 2008; 516: 4258-4266.

Ann J Materials Sci Eng - Volume 1 Issue 2 - 2014
ISSN : 2471-0245 | www.austinpublishinggroup.com
Whang et al. © All rights reserved

Citation: Teng-Yuan L, Yen-Jen W, Dean-Mo L and Wha-Tzong W. Surface Bio-Functionalization of a Novel High-Performance Hydrophilic Jeffamine-Modified Fluoro-Containing Polyimide for Biomedical Applications. Ann J Materials Sci Eng. 2014;1(2): 8.